

# Plate convergence at the westernmost Philippine Sea Plate

Wen-Nan Wu\*, Shu-Kun Hsu, Chung-Liang Lo, How-Wei Chen, Kuo-Fong Ma

*Institute of Geophysics, National Central University, No. 300, Jungda Rd., Chung-Li, 32001, Taiwan*

Available online 21 November 2007

## Abstract

To understand the convergent characteristics of the westernmost plate boundary between the Philippine Sea Plate (PSP) and Eurasian Plate (EP), we have calculated the stress states of plate motion by focal mechanisms. Cataloged by the Harvard centroid moment tensor solutions (Harvard CMT) and the Broadband Array in Taiwan (BATS) moment tensor, 251 focal mechanisms are used to determine the azimuths of the principal stress axes. We first used all the data to derive the mean stress tensor of the study area. The inversion result shows that the stress regime has a maximum compression along the direction of azimuth N299°. This result is consistent with the general direction of the rigid plate motion between the PSP and EP in the study area. In order to understand the spatial variation of the regional stress pattern, we divided the study area into six sub-areas (blocks A to F) based on the feature of the free-air gravity anomaly. We compare the compressive directions obtained from the stress inversion with the plate motions calculated by the Euler pole and the Global Positioning System (GPS) analysis. As a result, the azimuth of the maximum stress axis,  $\sigma_1$ , generally agrees with the directions of the theoretical plate motion and GPS velocity vectors except block C (Lanhsu region) and block F (Ilan plain region). The discrepancy of convergent direction near the Ilan plain region is probably caused by the rifling of the Okinawa Trough. The deviation of the  $\sigma_1$  azimuth in the Lanhsu region could be attributed to a southwestward extrusion of the Luzon Arc (LA) block between 21°N and 22°N whose northern boundary may be associated with the right-lateral NE–SW trending fault (i.e. Huatung Fault, HF) along the Taitung Canyon. Comparing the  $\sigma_1$  stress patterns between block C and block D, great strain energy along HF may not be completely released yet. Alternatively, the upper crust of block C may significantly have decoupled from its lower crust or uppermost mantle.

© 2007 Elsevier B.V. All rights reserved.

*Keywords:* Stress inversion; Luzon Arc; Philippine Sea Plate; Focal mechanism

## 1. Introduction

The westernmost Philippine Sea Plate (PSP) is converging toward the Eurasian Plate (EP) in the direction N310° (Seno et al., 1993) (Fig. 1). The associated westernmost plate boundary is located at the zone along the Luzon Arc (LA), which gradually evolves from normal subduction in the south to a mountain building collision in the north. The Taiwan orogen is generally considered as a result of the oblique collision between the LA and EP (e.g. Teng, 1987; Hsu and Sibuet, 1995; Wu et al., 1997; Sibuet and Hsu, 2004) (Fig. 1). With high-angle oblique thrust and left-lateral strike–slip components, the Longitudinal Valley fault in eastern Taiwan is considered as the plate suture zone (Yu and Kuo, 2001), or at least the Longitudinal Valley fault has consumed half of the convergent rate. Composed of the strato-volcanoes and trending approxi-

mately in the N–S direction, the 1200 km long LA has been formed due to the east-dipping subduction of the South China Sea basin along the Manila Trench.

Yu et al. (1999) have processed the Global Positioning System (GPS) data to study the crustal deformation and motion of the LA with respect to Eurasia and found that there is a significant southward increase in crustal motion along the N–S trend of the LA. Kao et al. (2000) used the bathymetry, seismicity, and source parameters of earthquakes to characterize the transition from oblique subduction to regional collision. To the south of 21°N, the feature of a subduction zone is clearly marked by both bathymetry and seismicity, while to the north of 23°N, the collision is the major mechanism with strong deformation on both sides of the suture. In between, the transition is accommodated by a distributed thrust deformation zone.

To date, the relationship among spatial distribution of the tectonic stress field, GPS velocity vectors and plate motion model of the westernmost PSP is still not clear. In this study, we

\* Corresponding author. Tel.: +886 3 4227151x65625; fax: +886 3 4222044.  
E-mail address: [wennan.v.wu@gmail.com](mailto:wennan.v.wu@gmail.com) (W.-N. Wu).

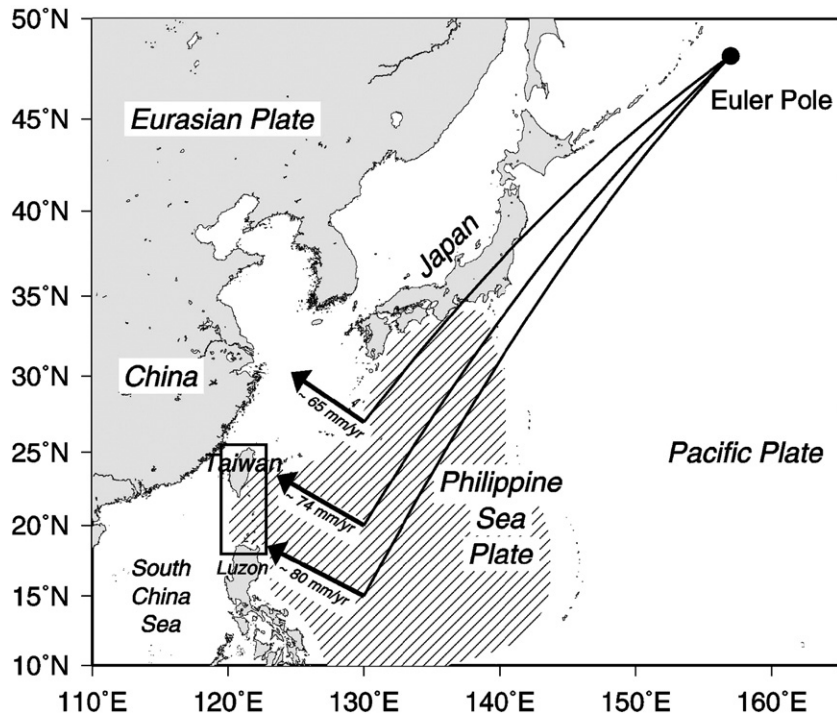


Fig. 1. The tectonic setting of Taiwan and Luzon region. The study area is marked by the rectangle. The Euler vectors (black arrows) show the plate motion of the PSP relative to the EP. Results were calculated from the Euler pole published by Seno et al. (1993).

attempt to investigate the variation of stress and the plate convergent characteristics of the westernmost PSP relative to the EP.

## 2. Method and data

### 2.1. Stress inversion method

Studying the state of stress in the Earth's crust and upper mantle is useful to understand the plate motion and regional deformation (Hardebeck and Hauksson, 2001; Xu, 2004). Earthquakes are indicators of stress; thus, we will use earthquake focal mechanisms to detect the stress state of convergent boundary which cannot be directly measured. Several authors have proposed methods to determine the orientations of stress axes of seismotectonic regime in spite of complicated tectonic settings (e.g. Gephart and Forsyth, 1984; Michael, 1984; Angelier, 1989; Horiuchi et al., 1995). In this study, we use the Focal Mechanisms Stress Inversion (FMSI) method of Gephart and Forsyth (1984) to determine the orientations of the principal stress axes between the westernmost PSP and EP.

FMSI method has three basic assumptions (Gephart and Forsyth, 1984; Gephart, 1990; Lu et al., 1997): (1) slip on the fault plane occurs in the direction of resolved shear stress; (2) the stress orientation is uniform in the calculated area; and (3) earthquakes are due to shear dislocations and can occur on preexisting faults. The FMSI method uses a grid search over stress field parameter space to find the best-fitting model that minimizes the average of the individual misfits between pos-

sible models and data (Gephart and Forsyth, 1984; Gephart, 1990).

The individual misfit calculated for each earthquake is defined as the smallest rotation angle about an axis of any orientation that would bring the slip direction into alignment with the resolved shear stress on the faults plane (Gephart and Forsyth, 1984). Fault plane ambiguity is addressed by using the nodal plane with the smaller misfit. In addition, the 95% confidence region is used to evaluate the quality of inversion (e.g. Gephart and Forsyth, 1984; Gillard et al., 1996; Lu et al., 1997). We obtained the azimuths and plunges of the three principal stresses axes  $\sigma_1$ ,  $\sigma_2$  and  $\sigma_3$  ( $\sigma_1 \geq \sigma_2 \geq \sigma_3$ ) and the ratio  $R = (\sigma_2 - \sigma_1) / (\sigma_3 - \sigma_1)$  ( $0 \leq R \leq 1$ ) by the best-fitting model. The value of  $R$  is a magnitude ratio of the intermediate principal stress ( $\sigma_2$ ) relative to the maximum ( $\sigma_1$ ) and minimum ( $\sigma_3$ ) principal stresses, and this may help us to distinguish the stress field type.

There are four stress parameters ( $\sigma_1$ ,  $\sigma_2$ ,  $\sigma_3$  and  $R$ ) in the inversion algorithm, and the minimum number of events used to inversion is four. Moreover, diverse data set can give better constrains to find out the stress tensor orientation. For above reasons, we used all the earthquake focal mechanisms within each data set to obtain an average local stress field without separating the fault types in a region.

The procedure to determine best-fitting stress model is as follows. We first perform a coarse initial grid search ( $10^\circ$  spacing in stress orientations) covering the whole range of possible models for each data set by the approximate method FMSIA (Gephart and Forsyth, 1984). We then take the best resulting stress model as a starting stress model to perform a fine

grid search ( $5^\circ$  spacing in stress orientations) by the exact method FMSIE (Gephart and Forsyth, 1984).

The size of the average misfit ( $\theta$ ) corresponding to the best-fitting stress model could be an indicator of how good the assumption of the uniform stress is made. According to a series of tests, carried out by Wyss et al. (1992) and Gillard et al. (1996), for the real earthquake focal mechanisms with errors of  $15^\circ$  (average of the uncertainties in strike, dip and rake) cannot obtain the average misfit of the stress inversion larger than  $6^\circ$ , thus the average misfit smaller than  $6^\circ$  may represent a homogeneous stress field. In contrast, the average misfit larger than  $9^\circ$  could be attributed to stress heterogeneity. The average misfit in the range between  $6^\circ$  and  $9^\circ$ , the stress solution is acceptable, but may reflect some heterogeneity (e.g. Wyss and Lu, 1995; Lu and Wyss, 1996; Lu et al., 1997).

## 2.2. Earthquake data

In order to investigate the stress regime of the LA in detail, we used the fault plane solutions from global data set and regional seismic data catalog. We searched the focal mechanism data from Harvard centroid moment tensor solutions (Harvard CMT) (Dziewonski et al., 1981) that occurred in our study area for the period from 1977 to 2004. The previous studies have shown that the discrepancy in the orientation of P and T axes of the reported Harvard CMT catalog is estimated to be less than  $15^\circ$  (e.g. Helffrich, 1997, Frohlich and Davis, 1999). This meets the criterion of high data quality requested as mentioned above. For this reason, we used the all events reported by Harvard CMT.

Additionally, we searched the earthquake focal mechanisms from the Broadband Array in Taiwan for Seismology (BATS) (Kao et al., 1998a). The BATS provided seismic moment solutions since 1995; however, in order to reduce the error of the stress inversion we searched the earthquakes from 1999 to 2002 with the average uncertainties of strike, dip and rake angles less  $15^\circ$ . The distribution of the epicenters is shown in Fig. 2.

In order to resolve the crustal stress field, the earthquakes with focal depth shallower than 35 km are adopted in the analysis. When both catalogs contain a same earthquake event, the BATS solution is used. In total, 251 fault plane solutions are used to investigate the stress field at the westernmost PSP. The focal mechanisms of the used earthquake are shown in Fig. 3a and b.

## 3. Theoretical plate motion and GPS estimated crustal motion

To understand the plate motion at the westernmost PSP, we calculated the directions of the relative plate motion based on the PH-EU plate model of Seno et al. (1993), which has been widely used to show the relative plate motion between the northern LA and the southeast Eurasian continental margin (e.g. Hsu, 2001a; Yu et al., 1999) (Table 1; Fig. 4). Hereafter, we refer the plate motion estimated by the PH-EU relative plate model to the theoretical plate motion. The directions of the theoretical plate motion range from  $N306.3^\circ$  to  $N310.3^\circ$  and the

velocities are in the range of 71.9 to 79.2 mm/yr from south to north in our study area.

In addition to the theoretical plate motion, we also calculate the crustal motion measured by the GPS data. The GPS data used to calculate the velocity field are from Yu et al. (1997); Yu et al. (1999) and Yu and Kuo (2001). The GPS velocity vectors of Yu et al. (1999) in the Taiwan–Luzon region from 1996 to 1998 used the reference site of Shanghai GPS station. On the other hand, the GPS observations for the crustal motion in the Taiwan island from 1990 to 1995 (Yu et al., 1997) and the Longitudinal Valley from 1992 to 1999 (Yu and Kuo, 2001) are

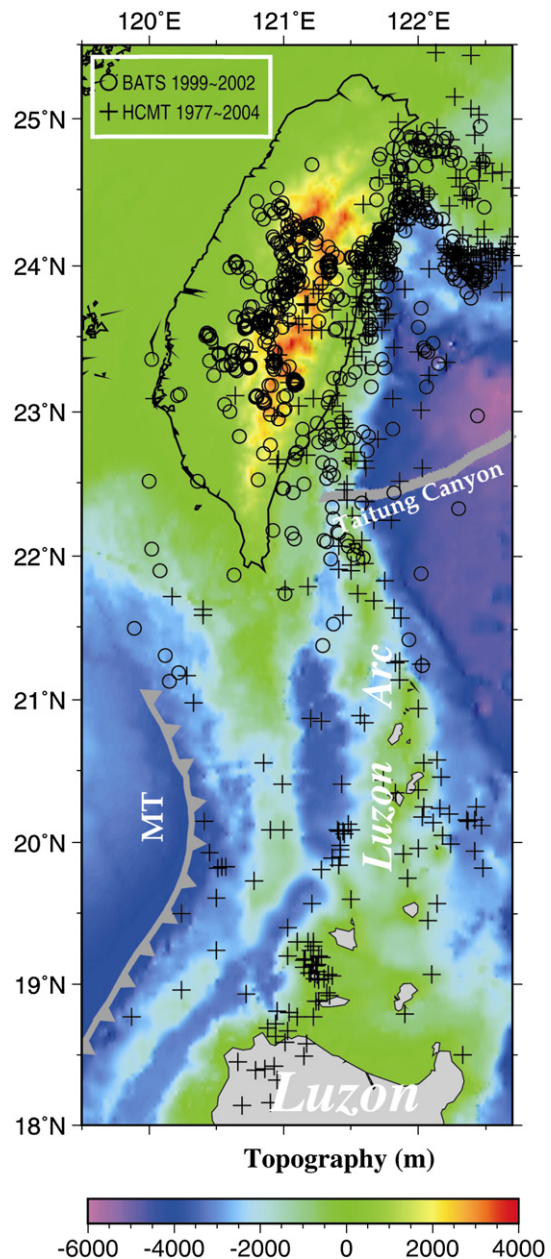


Fig. 2. The distributions of epicenters in the Taiwan–Luzon region. The MT denotes the Manila Trench. The crosses are the published Harvard CMT solutions from 1977 to 2004. The circles are the published BATS moment tensor solutions from 1999 to 2002. Along Taitung Canyon, the 8 mm/yr right-lateral NE–SW trending fault, Huatung Fault (HF), is suggested (Hsu, 2001).

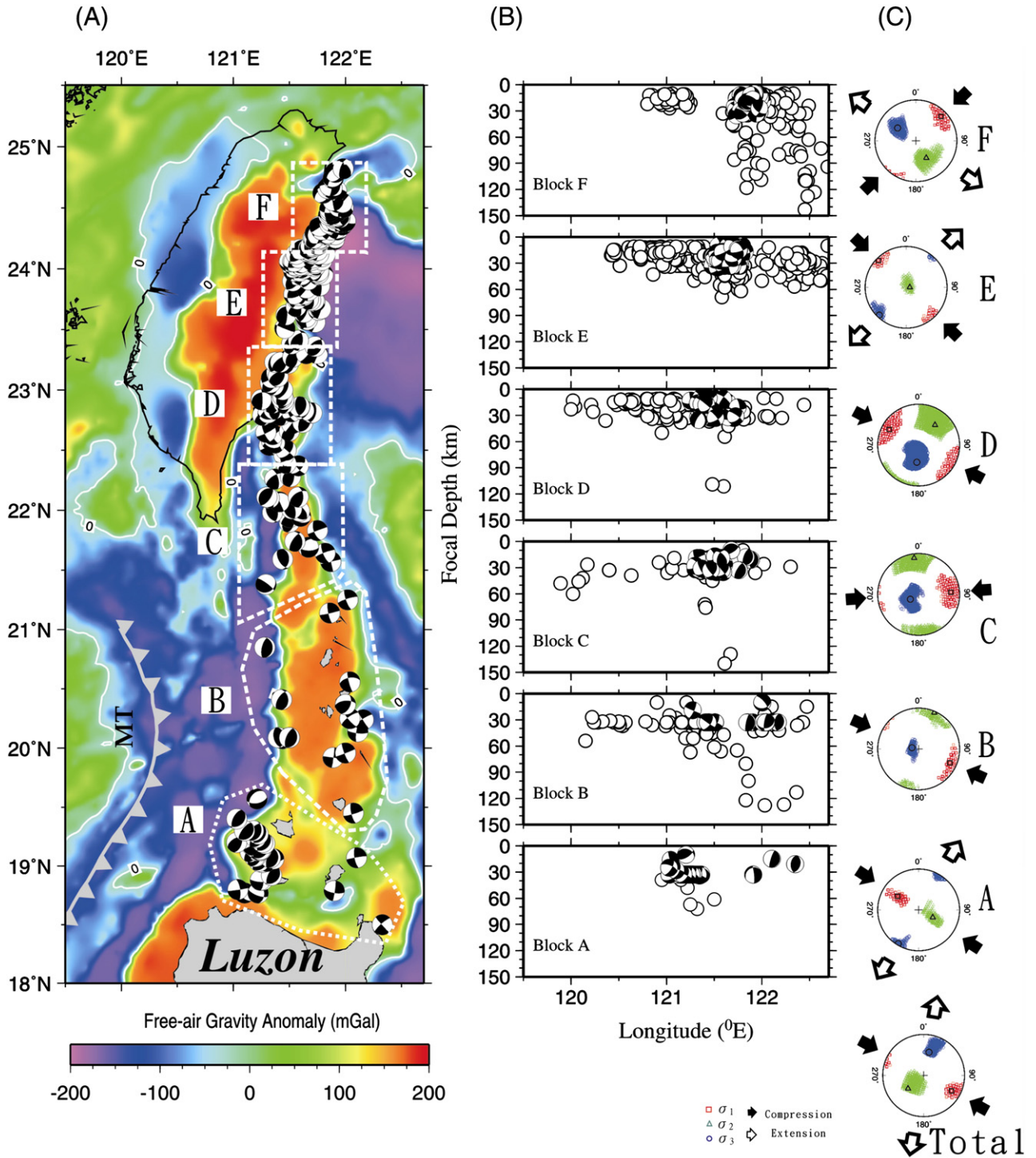


Fig. 3. The spatial distribution of the used earthquake events and the results of the stress inversion for each block. Based on spatial variation of the free-air gravity anomaly, the study area is divided into six subsets (blocks A to F). The focal mechanisms (A) and the depth distributions (B) of individual event within each block are highly correlated with the tectonic regimes based on distribution of free-air anomaly. The focal depths of all events are less than 35 km and are used as constrain for stress inversion. Background hypocenters (open circles) and focal spheres are projected both onto the surface (A) and a representative depth section for each block (B). (C) Major stress axes displayed through lower hemisphere projection with their orientation to within 95% confidence. The principal compressional and extensional stress axes for each block are denoted by solid and open arrows respectively. The result of using the whole data to perform the stress inversion is denoted as “Total” shown at the bottom.

relative to Paisha (Penghu island) GPS station which is situated on the Chinese continental margin. To have a consistent reference, we transformed all the velocity vectors to the values relative to Shanghai GPS station located in the stable EP.

It is noticed that on September 5, 1996, a major earthquake ( $M_L=7.1$ ) occurred near Lanhsu, and significant coseismic deformation was observed (Yu et al., 1999). The velocity before the earthquake (S102a) is about 68.2 mm/yr in the direction

Table 1  
Theoretical plate motion vectors; theoretical plate motions of entire subset estimated from the PH-EU plate model of Seno et al. (1993)

Point	Lat. (°N)	Lon. (°E)	Velocity (mm/yr)	Azimuth (°)
A	19.10	121.60	79.15	306.25
B	20.31	121.80	77.40	306.99
C	21.65	121.60	75.84	308.10
D	22.91	121.45	74.35	309.18
E	23.70	121.63	73.15	309.74
F	24.50	121.90	71.85	310.28

N306°, and the velocity after the earthquake (S102b) is about 71.7 mm/yr in the direction N317°. In this study we ignore the effect of the large earthquake, so we take the average value of S102a and S102b as the velocity of S102 station (i.e. N311.5° and 69.5 mm/yr). All GPS velocity vectors relative to Shanghai GPS station are listed in Table 2 and shown in Fig. 4.

#### 4. Results of the stress inversions

##### 4.1. Average stress pattern of the study region

To study the stress regime associated with the relative motion of the LA, we carried out the stress inversion procedures in two steps. The first one is to use all the available data as a whole data set and to calculate the best-fitting stress model. In the second step, we divide the data set into six subsets (blocks A to F), from south to north, to find the local variation from the regional stress pattern where the block division is based on the spatial variation of free-air gravity anomaly (Hsu et al., 1998) (Fig. 3a) where distinct features can be visually identified.

Note that the FMSI algorithm assumes that the value of the average misfit is mainly attributed to the heterogeneity of the tectonic stress field and errors of the fault plane solutions (Gillard et al., 1996; Lu et al., 1997). Because the average errors in strike, dip and rake of fault plane solutions are all less than 15°, we consider that the average misfit larger than 6° are due to the tectonic heterogeneity. In other words, the average misfit can reflect the degree of the tectonic homogeneity.

The result of best-fitting stress model is listed in Table 3. The best-fitting stress solutions with 95% confidence limits in each block are presented by lower hemisphere projection in Fig. 3c. Our results of the stress inversion are well constrained because the 95% confidence regions of  $\sigma_1$ ,  $\sigma_2$  and  $\sigma_3$  are not overlapped.

Firstly, we used the whole data to invert the stress tensor and obtain a well-constrained result (Table 3; Fig. 3c). The azimuth of  $\sigma_1$  is N299° and it is consistent with the GPS-based velocity of Yu et al. (1999) and the Euler vector of the PSP predicted by Seno et al. (1993). Based on this result, we conclude that the overall azimuth of  $\sigma_1$  in our study area may account for the crustal motion of the LA (or PSP) relative to the EP. However, the average misfit is up to 10.15°. This suggests that the stress field in our study area is heterogeneous to some extent. It is not surprising because the western boundary of the PSP consists of different seismogenic units and tectonic regimes as mentioned previously.

##### 4.2. Variation of the stress field

As shown in Fig. 3a and b, six subsets of the study area are defined based on the spatial variation of free-air gravity anomaly (Hsu et al., 1998). We performed the stress inversion for each subset in the same way as for the whole data. The results are shown in the Table 3 and Fig. 3c.

In terms of the azimuth of  $\sigma_1$ , the stress inversions show rather similar results for all subsets except for blocks C and F (Table 3; Figs. 3c and 4). Most of the azimuths of  $\sigma_1$  fall in the range of N294° to N314° and the plunges in the range of 5° to 35°. There are three subsets (blocks B, C and D) whose axes of  $\sigma_3$  are in the vertical direction, indicating dominant thrust-type stress fields. In contrast, blocks A and E have the axes of  $\sigma_2$  in the vertical direction, indicating strike-slip-type stress fields. These phenomena suggest that there could be a significant crustal discontinuity between block D and block E as suggested by Hsu (2001b). Likewise there could be a crustal discontinuity between block A and block B.

For blocks A, B and E the azimuths of  $\sigma_1$  generally agree with the directions calculated by GPS study (Yu et al., 1999) (Fig. 4a). Each of those regions has misfits less than 6°, suggesting that the stress field in each region can be deemed as homogenous. In contrast, for blocks C (Lanhsu region) and F (Ilan plain region), the azimuths of  $\sigma_1$  are significantly different from the others (Figs. 3c and 4). The result for block F can be attributed to tectonic complexity associated with the oblique subduction of the PSP and the opening process of the Okinawa Trough (Yu et al., 1997; Sibuet et al., 1998; Kao et al., 1998b; Hsu, 2001b). On the other hand, blocks D and F show their misfits larger than 6°, indicating that the stress fields are rather heterogeneous inside the blocks.

#### 5. Southwestward migration of the Luzon Arc block between 21°N and 22°N

As a result of our stress inversion at the westernmost PSP, the mean azimuth of  $\sigma_1$  of the PSP relative to the EP is N299°. However, we can discern the heterogeneous character of the plate convergence from the subset stress pattern analysis along the LA. It is especially remarkable that the azimuth of  $\sigma_1$  of block C displays at least 30° rotation in azimuth less than other blocks, except for the Ilan plain block (Fig. 4).

Basically, the GPS surveys can indicate the motion of the upper crust, while the global plate motion model suggests the motion of a rigid plate. If we examine the surface crustal motion by the GPS survey and the plate motion of the PH-EU plate model in our study area (Tables 1 and 2; Fig. 4), we can find different plate convergent directions from the GPS velocity vectors and the plate motion model, respectively. The GPS velocity vectors are generally consistent with the theoretical plate motion in the southern part, while in the northern part of the study area, the crust gradually rotates clockwise from south to north (e.g. Lee et al., 1991). This rotation indicates that upper crust is more or less decoupled from the lower crust or upper mantle in the Taiwan–Luzon region. The deviation in the upper crustal motion could be associated with the active mountain

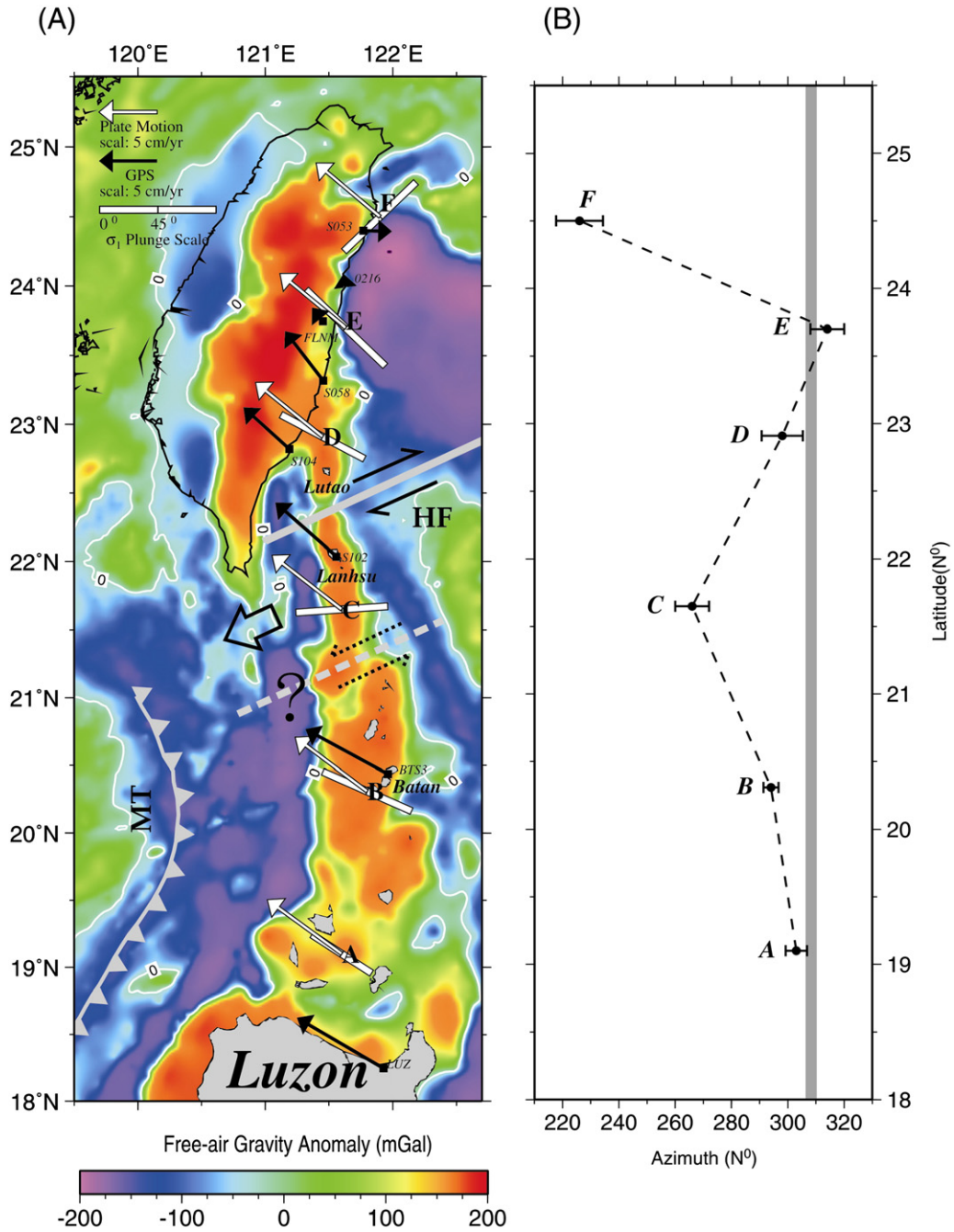


Fig. 4. (A) Comparison of the  $\sigma_1$  direction (white bars), theoretical plate motion (white arrows) and GPS velocity vectors (black arrows). The MT represents the Manila Trench, and the HT denotes the Huatung Fault. The scales are shown on upper left corner. The length of a white bar indicates the plunge scale for each  $\sigma_1$ . (B) The estimated azimuth of the  $\sigma_1$  for each specified block. The error bar is estimated by the average misfit value. The gray zone indicates the theoretical plate motion directions of the PSP relative to EP. Note that in block C and block F the estimated azimuths of the  $\sigma_1$  have anomalous deviations.

building collision in Taiwan and the rifting in the Okinawa Trough area. In other words, the plate motion model may predict the direction of rigid plate motion in a large scale, but it fails to predict the local and complex crustal portion. Moreover, the GPS survey may just express the local and surface crustal motion.

Because the used earthquakes with the focal depths extend to 35 km, the directions of compression could be closer to the prediction of the theoretical plate motion. For this reason, we compare the plate convergence directions between our results

and the theoretical plate motion. For blocks A and B, the small average misfit ( $3.83^\circ$  and  $2.67^\circ$ ), and the azimuths of  $\sigma_1$ , GPS and theoretical plate motion are consistent with each other (Fig. 4a). As mentioned previously, blocks C and F display larger differences of the azimuths of  $\sigma_1$  relative to the theoretical plate motion. The discrepancy of block F, in the northernmost area, is explained explicitly by distinctive rifting of the Okinawa Trough. For block C, the azimuth of  $\sigma_1$  deviates  $40^\circ$  anticlockwise from the theoretical plate motion. To the north and south of block C the azimuths of  $\sigma_1$  are generally consistent

Table 2  
GPS velocity vectors relative to Shanghai GPS station located in the stable EP

Station	Lat. (°N)	Lon. (°E)	Velocity (mm/yr)	Azimuth (°)	Reference
BTS3	20.438	121.963	80.7	298.6	Yu et al. (1999)
S102	22.037	121.558	70.0	311.5	Yu et al. (1999)
S104	22.821	121.189	53.3	312.5	Yu et al. (1999)
S058	23.319	121.454	53.6	322.6	Yu et al. (1999)
FLNM	23.746	121.453	15.2	321.3	Yu et al. (1999)
O216	24.025	121.623	7.8	352.0	Yu and Kuo (2001)
S053	24.399	121.770	24.2	91.4	Yu et al. (1997)

with the theoretical plate motion. To explain the discrepancy in azimuth of  $\sigma_1$  of block C, we suggest that the area between 21°N and 22°N of our study region (including block C) could migrate southwestward. As indicated by Hsu (2001a), a large right-lateral NE–SW Huatung Fault (HF), located at the Huatung Basin and along part of Taitung Canyon, could extend southwestward and bisect the Lutao and Lanhsu arc segments (Fig. 4a). The faulting along the Taitung Canyon was first reported by Hsu et al. (1996) and was elaborated by Kao et al. (2000) as the Taitung Canyon Fault Zone.

Taking into account the southwestward migration of block C along the trend of the HF, the plate convergence of the PSP relative to the EP should be more counterclockwise. Based on the GPS result, the relative motion along the HF is about 8 mm/yr (Hsu, 2001a). However, this situation could only change the plate convergence of block C to the azimuth of N305°, instead of the calculated stress inferred N266° (Fig. 5). When considering the azimuth of  $\sigma_1$  of block C (N266°) as the observed convergence direction, the relative motion between blocks C and D along the HF (azimuth N245°) must be 138 mm/yr which is far larger than 8 mm/yr (Fig. 5). This result may imply two scenarios. Firstly, a great strain energy release of the crustal, strike–slip faulting along HF is expected. Secondly, the decoupling of the upper crust from the lower crust and the uppermost mantle is suggested, so that they can display different degrees of southwestward motion. Additionally, block C may vertically rotate clockwise looking from the south, which might explain the different amount of crustal GPS observations. However, based on the historical great earthquake faulting (e.g. Wu, 1978; Sibuet et al., 2004),

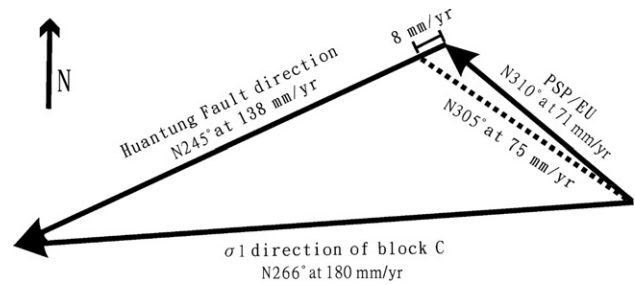


Fig. 5. The kinematical model for block C (the Lanhsu islet region). PSP/EU presents the relative motion between the PSP and EP. See text for detail discussion.

great strike–slip earthquakes along the HF in the direction of N245° can occur again.

## 6. Conclusion

Based on the stress inversion of earthquake focal mechanisms, we have obtained a mean azimuth of N299° for the plate convergence direction between the westernmost PSP and EP. This result is consistent with the direction of the relative motion between the PSP and EP predicted by the PH-EU plate motion model. However, different segmental block of the westernmost PSP could have different plate convergent directions. The plate convergence at the westernmost PSP is strongly associated with tectonic settings. Thus, it is not a rigid plate convergence between the westernmost PSP and EP. The westernmost PSP generally follows the predicted plate motion except for block C. The large deviation of plate convergent direction of block C is ascribed to a southwestward migration of block C of the westernmost PSP. However, a large component of strain energy of strike–slip faulting along the northern boundary of block C (or along the HF) seems not to be released yet or the upper crust and lower crust of block C has decoupled to some extent. Comparing the crustal GPS motion, the theoretical plate motion and our results suggest that south of about 21°N the westernmost PSP displays a normal plate convergence of the South China Sea basin beneath the LA, while north of 22°N, the plate convergence is expressed in response to the mountain building collision.

Table 3  
Orientation of principal stresses inverted from fault plane solutions (FPS) of the westernmost PSP

Block	Number of FPS	$\sigma_1$		$\sigma_2$		$\sigma_3$		R value	Misfit ( $\theta$ )
		Azimuth	Plunge	Azimuth	Plunge	Azimuth	Plunge		
Total	251	119	20	230	45	13	38	0.6	10.150
A	32	303	35	118	55	211	3	0.3	3.826
B	16	114	15	23	3	281	75	0.3	2.672
C	21	86	19	353	9	240	69	0.3	6.022
D	38	298	17	39	33	186	52	0.6	7.361
E	76	314	5	89	82	224	5	0.5	5.984
F	68	46	13	149	46	305	41	0.5	8.315

$\sigma_1$  — maximum compressive stress;  $\sigma_2$  — intermediate compressive stress;  $\sigma_3$  — minimum compressive stress; R — magnitude ratio of principal stresses (see in the text).

## Acknowledgments

We are grateful to Ruey-Juin Rau, Wen-Tzong Liang, Ya-Ju Hsu for the discussion to use the BATS and GPS data, and Chung-Pai Chang for the plentiful discussions. W.-N. Wu would like to thank John Gephart for making his program available and Hsin-Chiang Liang for helping to compile the computer code. The significant comments from two anonymous reviewers are appreciated. The figures were prepared with the GMT software (Wessel and Smith, 1998). This study was supported under a grant from National Science Council, Taiwan, R.O.C.

## References

- Angelier, J., 1989. From orientation to magnitudes in paleostress determination using fault slip data. *J. Struct. Geol.* 11, 37–50.
- Dziewonski, A.M., Chou, T.-A., Woodhouse, J.H., 1981. Determination of earthquake source parameters from waveform data for studies of global and regional seismicity. *J. Geophys. Res.* 86, 2825–2852.
- Frohlich, C., Davis, S.D., 1999. How well constrained are the well-constrained T, B, and P axes in moment tensor catalogues? *J. Geophys. Res.* 104, 4901–4910.
- Gephart, J.W., Forsyth, D.W., 1984. An improved method for determining the regional stress tensor using earthquake focal mechanism data: application to the San Fernando earthquake sequence. *J. Geophys. Res.* 89, 9305–9320.
- Gephart, J.W., 1990. FMSI: A FORTRAN program for inverting fault/slickenside and earthquake focal mechanism data to obtain the original stress tensor. *Comput. Geosci.* 16, 953–989.
- Gillard, D., Wyss, M., Okubo, P., 1996. Type of faulting and orientation of stress and strain as a function of space and time in Kilauea's south flank, Hawaii. *J. Geophys. Res.* 101, 16025–16042.
- Hardebeck, J.L., Hauksson, E., 2001. Stress orientations obtained from earthquake focal mechanisms: what are appropriate uncertainty estimates? *Bull. Seism. Soc. Am.* 91, 250–262.
- Helffrich, G.R., 1997. How good are routinely determined focal mechanisms empirical statistics based on a comparison of Harvard, USGS and ERI moment tensors? *Geophys. J. Int.* 131, 741–750.
- Horiuchi, S., Russo, G., Hasegawa, A., 1995. Discrimination of fault planes from auxiliary planes based on simultaneous determination of stress tensor and a large number of fault plane solutions. *J. Geophys. Res.* 100, 8327–8338.
- Hsu, S.-K., 2001a. Subduction/collision complexities in the Taiwan–Ryukyu junction area: tectonics of the northwestern corner of the Philippine Sea Plate. *Terr. Atmos. Oceanic Sci.* 209–230 Suppl. Issue.
- Hsu, S.-K., 2001b. Lithospheric structure, buoyancy and coupling across the southernmost Ryukyu subduction zone: an example of decreasing plate coupling. *Earth Planet. Sci. Lett.* 186, 471–478.
- Hsu, S.-K., Sibuet, J.-C., 1995. Is Taiwan the result of arc–continent or arc–arc collision? *Earth Planet. Sci. Lett.* 136, 315–324.
- Hsu, S.-K., Sibuet, J.-C., Shyu, C.-T., Liu, C.-S., 1996. Transition between the Okinawa trough backarc extension and the Taiwan collision: new insights on the southernmost Ryukyu subduction zone. *Mar. Geophys. Res.* 18, 163–187.
- Hsu, S.-K., Liu, C.-S., Shyu, C.-T., Liu, S.-Y., Sibuet, J.-C., Lallemand, S., Wang, C., Reed, D., 1998. New gravity and magnetic anomaly map in the Taiwan–Luzon region and their preliminary interpretation. *Terr. Atmos. Oceanic Sci.* 9, 509–532.
- Kao, H., Jian, P.-R., Ma, K.-F., Huang, B.-S., Liu, C.-C., 1998a. Moment-tensor inversion for offshore earthquakes east of Taiwan and their implications to regional collision. *Geophys. Res. Lett.* 25, 3619–3622.
- Kao, H., Shen, S.J., Ma, K.-F., 1998b. Transition from oblique subduction to collision: earthquakes in the southernmost Ryukyu arc–Taiwan region. *J. Geophys. Res.* 103, 7211–7229.
- Kao, H., Huang, G.-C., Liu, C.-S., 2000. Transition from oblique subduction to collision in the northern Luzon arc–Taiwan region: constraints from bathymetry and seismic observations. *J. Geophys. Res.* 105, 3059–3079.
- Lee, T.-Q., Kissel, C., Barrier, E., Laj, C., Chi, W.-R., 1991. Paleomagnetic evidence for a diachronic clockwise rotation of the Coastal Range, eastern Taiwan. *Earth Planet. Sci. Lett.* 104, 245–257.
- Lu, Z., Wyss, M., 1996. Segmentation of the Aleutian plate boundary derived from stress direction estimates based on fault plane solutions. *J. Geophys. Res.* 101, 803–816.
- Lu, Z., Wyss, M., Pulpan, H., 1997. Details of stress directions in the Alaska subduction zone from fault plane solutions. *J. Geophys. Res.* 102, 5385–5402.
- Michael, A.J., 1984. Determination of stress from slip data: faults and folds. *J. Geophys. Res.* 89, 11517–11526.
- Seno, T., Stein, S., Gripp, A.E., 1993. A model for the motion of the Philippine Sea Plate consistent with NUVEL-1 and geologic data. *J. Geophys. Res.* 98, 17941–17948.
- Sibuet, J.-C., Hsu, S.-K., 2004. How was Taiwan created? *Tectonophysics*, 379, 159–181.
- Sibuet, J.-C., Deffontaines, B., Hsu, S.-K., Thureau, N., Le Formal, J.-P., Liu, C.-S., ACT party, 1998. Okinawa trough backarc basin: early tectonic and magmatic evolution. *J. Geophys. Res.* 103, 30245–30267.
- Sibuet, J.-C., Hsu, S.-K., Normand, A., 2004. Tectonic significance of the Taitung Canyon, Huatung Basin, east of Taiwan. *Marine Geophys. Res.* 25, 95–107.
- Teng, L.S., 1987. Stratigraphic records of the late Cenozoic Penglai Orogeny of Taiwan. *Acta. Geol. Taiwanica* 25, 205–224.
- Xu, P.L., 2004. Determination of regional stress tensors from fault–slip data. *Geophys. J. Int.* 157, 1316–1330.
- Wessel, P., Smith, W.M.F., 1998. New improved version of generic mapping tools released. *EOS Trans.* 79, 579 AGU.
- Wu, F.T., 1978. Recent tectonics of Taiwan. *J. Phys. Earth* 26 (suppl.), S265–S299.
- Wu, F.T., Rau, R.-J., Salzberg, D., 1997. Taiwan orogeny: thin skinned or lithospheric collision? *Tectonophysics* 274, 191–220.
- Wyss, M., Lu, Z., 1995. Plate boundary segmentation by stress directions: southern San Andreas fault, California. *Geophys. Res. Lett.* 22, 547–550.
- Wyss, M., Liang, B., Tanigawa, W.R., Wu, X., 1992. Comparison of orientations of stress and strain tensors based on fault plane solutions in Kaoiki Hawaii. *J. Geophys. Res.* 97, 4769–4790.
- Yu, S.-B., Kuo, L.-C., 2001. Present-day crustal motion along the Longitudinal Valley Fault, eastern Taiwan. *Tectonophysics* 333, 199–217.
- Yu, S.-B., Chen, H.-Y., Kuo, L.-C., 1997. Velocity field of GPS stations in the Taiwan area. *Tectonophysics* 274, 41–59.
- Yu, S.-B., Kuo, L.-C., Punongbayan, R.S., Ramos, E.G., 1999. GPS observation of crustal motion in the Taiwan–Luzon region. *Geophys. Res. Lett.* 26, 923–926.